# AXON EXTRACTION FROM FLUORESCENT CONFOCAL MICROSCOPY IMAGES

*Alejandro Mottini, Xavier Descombes and Florence Besse*

Project Morpheme, INRIA/I3S/IBDC, 2000 Route des Lucioles, 06903 Sophia Antipolis Cedex, France

## ABSTRACT

The morphological analysis of axonal trees is an important problem in neuroscience. The first step for such an analysis is the extraction of the axon. Due to the high volume of generated image data and the tortuous nature of the axons, manual processing is not feasible. Therefore, it is necessary to develop techniques for the automatic extraction of the neuronal structures. In this paper we present a new approach for the automatic extraction of axons from fluorescent confocal microscopy images. It combines algorithms for filament enhancement, binarization, skeletonization and gap filling in a pipeline capable of extracting the axons. The performance of the proposed method was evaluated on real images. Results support the potential use of this technique in helping biologists perform automatic extraction of axons from fluorescent confocal microscopy images.

***Index Terms*—** axon extraction, fluorescent confocal microscopy, Gabor functions, tensor voting

## 1. INTRODUCTION

Biologists currently utilize different imaging techniques capable of producing images of biological systems at a cellular or subcellular level. Among them is confocal microscopy, a technique capable of generating sharp 3D images of thick specimens at very high resolutions. This imaging system provides an efficient way of analyzing supra-cellular structures.

It is known that their precise morphology provides information on their functioning and allows the characterization of pathological states. Therefore, the analysis of the morphological differences between normal and pathological structures is of paramount importance. In particular, the analysis of neuronal axonal topologies allows biologists to study the causes of neurological diseases such as Fragile X Syndrome and Spinal Muscular Atrophy.

For this purpose, biologists have labeled single neurons within intact adult Drosophila fly brains and have acquired 3D fluorescent confocal microscopy images of their axonal trees. Both normal neurons and neurons in which certain genes related to neurological diseases in humans were inactivated have been imaged (see Figure 1).

In order to perform the morphological analysis of the axons, it is first necessary to segment them. Therefore, the images need to be processed and analyzed.

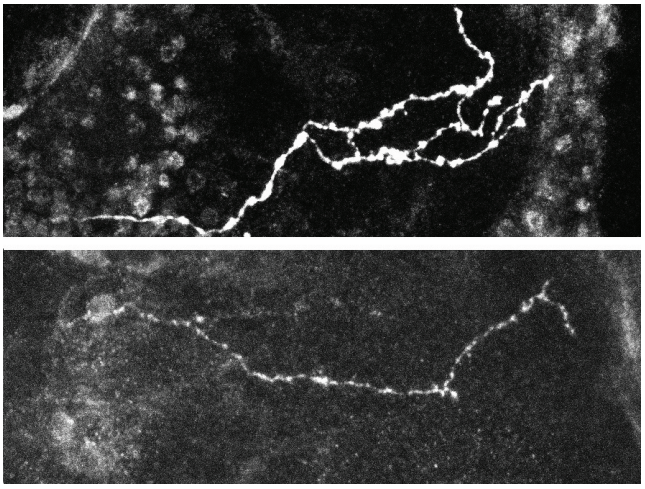


**Fig. 1**: Normal (top) and mutant (bottom) axons (maximum intensity projections).

Due to the high volume of image data (on average, each image has a size of $1024 \times 1024$ pixels by 16 layers) and the tortuous nature of the axons, manual processing is not feasible. It is thus necessary to develop techniques for the automatic extraction and analysis of these neuronal structures.

Currently, many methods for axon extraction can be found in the literature. Some, such as [1, 2, 3] concentrate on, given a 3D image stack containing many axons (sometimes overlapping each other), segmenting each individual axon. In most cases these images contain many non-bifurcating axons, and their objective is to segment each of them. Since the axons overlap on occasions, the authors have to resort to strategies that lead to overcomplicated and computationally heavy algorithms. Moreover, many of these methods require the user to manually select the center of each axon in the first slice of the stack. This is not suited for automatically analyzing large databases of images, which is necessary if one intends to statistically compare different populations of axons.

Other methods such as [4] are limited to 2D images. This restricts their usefulness since a 2D analysis does not give crucial information on the axon's morphometry and topology. In particular, the lengths and bifurcation points in the 2D projection might be different to the original 3D image.

In addition, several computer applications (such as Neuromantic [1] and FeatureJ [2]) have been developed for the processing of this particular type of images (or similar ones). These applications, which include different extraction algorithms, provide manual or semi-automatic modes of operation along with friendly graphical user interfaces (GUI). These, however, require time consuming manual (or semi-automatic) tracing of the axon, obtain unacceptable results in our images and/or are restricted to the 2D case.

In this paper we propose a solution which combines algorithms for filament enhancement, binarization, skeletonization and gap filling in a pipeline capable of extracting axons from confocal microscopy images containing a single labelled neuron (we do not consider the more challenging case of multiple labelled neurons that intertwine and synapse). Furthermore, this method is designed to work on 3D image stacks. In the future, we intend to apply this technique to analyze the morphological differences between normal and mutant axons.

## 2. AXON EXTRACTION ALGORITHM

Our method applies several consecutive steps for extracting the axons: Filament Enhancement, Binarization, Skeletonization and Gap Filling.

The first step of the pipeline is filament enhancement. This is done with a multiscale filtering of the images based on Gabor functions. Due to the low resolution of our images in the axis perpendicular to the sections, we chose to work on each 2D slice independently. However, the analysis that follows can easily be extended to the 3D case.

We consider Gabor functions defined as follows:

$$G(x,y) = \cos\left(\frac{x_1\pi}{\sqrt{2}\lambda\sigma_g}\right)\exp\left(-\frac{x_1^2+\gamma^2 y_1^2}{2\sigma_g^2}\right) \tag{1}$$

where $x_1 = x\cos(\theta)+y\sin(\theta)$ and $y1 = x\sin(\theta)-y\cos(\theta)$. The parameters $\theta, \lambda, \sigma_g$ and $\gamma$ represent the orientation, wavelength, scale and aspect ratio respectively. If we consider the image $I(x,y)$, then the filtered image $F$ is defined as $F = \|G * I\|$. A high value of $F$ at a point $(x,y)$ for a given $\theta$ is evidence of local structure (axon) for that direction and position. To avoid false positives on edges, we consider two Gabor filters associated to each side of the filament (inside and outside):

$$G^+(x,y) = \begin{cases} \cos\left(\frac{x_1\pi}{\sqrt{2}\lambda\sigma_g}\right)\exp\left(-\frac{x_1^2+\gamma^2 y_1^2}{2\sigma_g^2}\right) & \text{if } x_1 > 0 \\ 0 & \text{otherwise} \end{cases} \tag{2}$$

$$G^-(x,y) = \begin{cases} \cos\left(\frac{x_1\pi}{\sqrt{2}\lambda\sigma_g}\right)\exp\left(-\frac{x_1^2+\gamma^2 y_1^2}{2\sigma_g^2}\right) & \text{if } x_1 < 0 \\ 0 & \text{otherwise} \end{cases} \tag{3}$$

The filtered image is then given by $F = \min(\|G^- * I\|, \|G^+ * I\|)$. The filters are also normalized to eliminate their dependency to the absolute intensity of the image. Finally, the filament enhancement filter is given by $F = \min(\|\Psi^- * I\|, \|\Psi^+ * I\|)$ where:

$$\Psi^-(x,y) = \begin{cases} \eta_-^- G^-(x,y) & \text{if } G^-(x,y) < 0 \\ \eta_-^+ G^-(x,y) & \text{if } G^-(x,y) \geq 0 \end{cases} \tag{4}$$

$$\Psi^+(x,y) = \begin{cases} \eta_+^- G^+(x,y) & \text{if } G^+(x,y) < 0 \\ \eta_+^+ G^+(x,y) & \text{if } G^+(x,y) \geq 0 \end{cases} \tag{5}$$

The constants $\eta_-^-, \eta_-^+, \eta_+^-$ and $\eta_+^+$ are obtained by the normalization of the two filters.

The different parameters involved in the filters are set by imposing certain conditions (such as a ratio of 3 between the length and the width of the filter and a filter value of 0 at the edges of the filaments). Therefore, the filter's parameters for filaments of width $n$ are given by:

$$\lambda = \frac{4}{3}, \sigma_g = \frac{3n}{4\sqrt{2}}, \gamma = \frac{1}{3} \tag{6}$$

To perform a multiscale analysis of the images, the parameter $n$ is varied between the expected widths of the axons. Apart from the Gabor filtering, we also tested two other filament enhancement filters found in the literature [5, 6]. However, we found that the proposed filter obtains better results for our images.

The next step in the extraction process is the binarization of the images. The threshold is automatically computed by decreasing Otsu's threshold [7] by a certain percentage (found empirically for our images). Afterwards, the binary image is skeletonized. The skeleton is used as a way of summarizing the geometrical and topological properties of the shape.

It is very common that, once the skeleton has been extracted, it presents discontinuities (gaps) due to the binarization in a noisy context. Several algorithms exist in the literature to solve this problem. In particular, we chose the method proposed in [8]. In this work, the authors propose a tensor voting approach for filling gaps in 3D micro-vascular networks. The algorithm is divided into four steps. The first step (referred to as segmentation) involves separating the skeleton segments (referred to as a tokens) into 3 categories:

- Island token: segments which are not connected to other segments or only connected from one side, and have a length of less that a given value (referred to as $\beta$).
- Segment token: segments which are either connected from both sides to other segments or have one or two free ends and length greater than $\beta$.
- Segment-end token : the last pixel of the free segment end for segments of length greater than $\beta$.

The second step is the creation of the tensor field $T$. It involves assigning to each point of the image a tensor (a 3x3 symmetric non-negative matrix). Each tensor depends on the contribution of all the tokens in the image:

$$T(i,j,k) = \sum_{n=1}^{N} TE_n(i,j,k) + \sum_{m=1}^{M} TI_m(i,j,k) + \sum_{q=1}^{Q} TS_q(i,j,k) \tag{7}$$

[1] http://www.reading.ac.uk/neuromantic/

[2] http://www.imagescience.org/meijering/software/featurej/

where $TE_n$ is the tensor field created by the $n^{th}$ segment-end token, $TI_m$ the one created by the $m^{th}$ island token and $TS_q$ the one created by the $q^{th}$ segment token. The calculation of these contributions depends on the type and properties of each token. For an island token centered at point $C$, the tensor generated at point $P$ of the image is given by:

$$TI = cp * cp, \qquad cp = \frac{CP}{\|CP\|} \exp\left(-\frac{\|CP\|^2}{\sigma_t^2}\right) \tag{8}$$

where $\sigma_t$ is a parameter of the algorithm. Let $O$ be a segment-end token (the end point of segment $S$), $P$ a point in the image and $V$ the tangent to segment $S$ in $O$. We then define vector $W = 2OP(OP.V) - V$. This vector is the oriented tangent at $P$ to the circle $C$ which contains $O$ and $P$ and which is tangent to $V$ at $O$. Then, the tensor $TE$ is defined as:

$$TE = w * w, \qquad w = \frac{W}{\|W\|} \exp\left(-\frac{r^2 + c\varphi^2}{\sigma_t^2}\right) \tag{9}$$

where $r$ is the length of the arc $\widehat{OP}$ of circle $C$, $\varphi$ its curvature and $c$ a parameter of the algorithm. Finally, the tensor field $TS$ associated to a segment token $S$ is defined as follows:

$$TS = np * np, \qquad np = \frac{NP}{\|NP\|} \exp\left(-\frac{(\|NP\|)^2}{\sigma_t^2}\right) \tag{10}$$

where $P$ is a point of the image and $N$ is the closest point of segment $S$ to the point $P$. The different parameters are set according to the author's recommendations in [8]. Both $\sigma_t$ and $c$ were fixed for all our experiments and are thus not user dependent.

The next step consists in generating a scalar vector field called the saliency map. For each point in the image, the value of the field is calculated by subtracting the eigenvalues of the tensor at this point (see Figure 2). The final step is the reconnection step. The algorithm reconnects the paths along the points with maximum saliency.

In order to improve the speed of the algorithm, a small modification was introduced. The tensor map is not computed for all voxels in the image. Instead, cones of user defined height and radius are generated on each end point. Next, the tensors are computed in these regions (the cones) only if other points belonging to the skeleton fall inside.

At the end of the extraction process, a connected component labeling is performed and only the largest one is kept. This component corresponds to the axon.

## 3. VALIDATION

The proposed technique was validated on a group of 12 real 3D images, each containing one axonal tree, different noise levels and tree complexities. These images were manually segmented by an experienced biologist and the results compared with the ones obtained by our algorithm. To quantitatively measure the quality of our results, the RMSE between the manual and the automatic tracings were computed. The results are summarized in Figure 7.

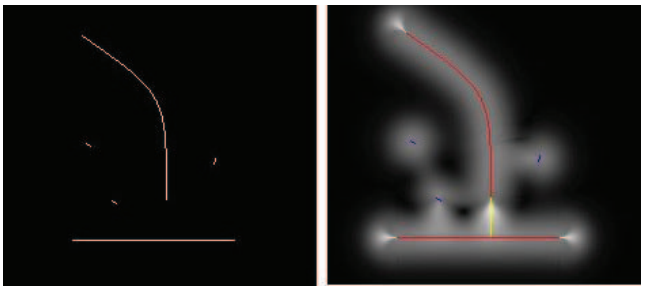


**Fig. 2**: Original image (left) and corresponding saliency map (right). The gap to be filled is marked in yellow.

Figure 3 shows the results obtained for the different filament enhancement filters. It can be appreciated that the proposed filter obtains better results for these types of images. Figure 4 shows the results obtained on each step of the pipeline for one image of the data set. It shows how the proposed method is able to extract the axons even on images with significant noise. Figure 5 compares our results with the manually constructed skeletons for two different cases. The figure shows how the axon extracted by our method is very similar to the one segmented by the biologist. However, on occasions they have short branches that are not present in the manual segmentations. We plan to solve this problem by adding a 3D skeleton pruning step in the algorithm. Figure 6 shows how the gap filling step is able to connect the gaps present in a skeleton. This step is very important since the skeletons usually present discontinuities.

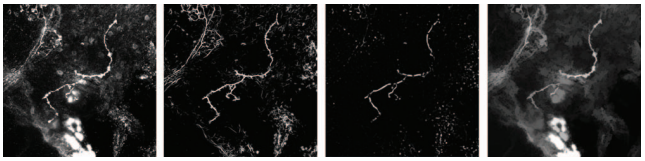


**Fig. 3**: Comparison between the Gabor filament enhancer and the methods proposed in [5, 6]: From left to right: original image, Gabor filtering, Frangi et al. and Wilkinson et al. (maximum intensity projections).

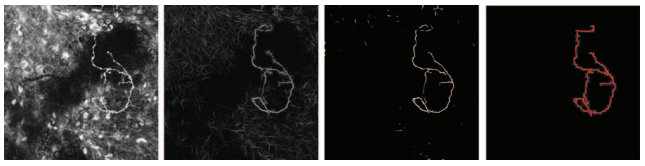


**Fig. 4**: Results obtained on each step of the algorithm for one image stack (maximum intensity projections). From left to right: original image, filament enhancement, binarization and final result.

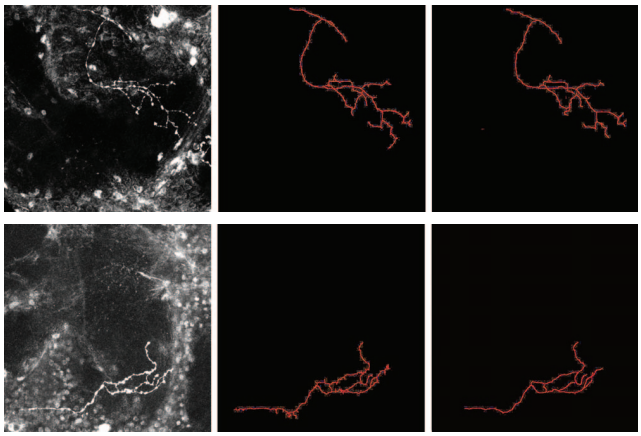


**Fig. 5**: Comparison between original image (left), our result (middle) and ground truth (right) for two images (maximum intensity projections).

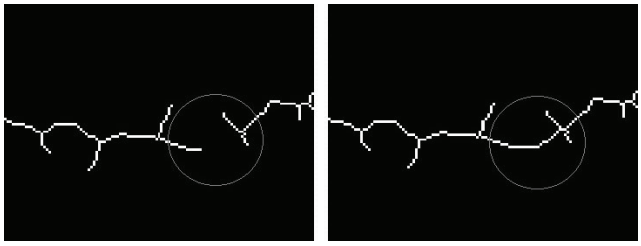


**Fig. 6**: Result before (left) and after (right) the gap filling step (maximum intensity projections). The gray circle marks the gap to be filled.

## 4. CONCLUSIONS

An algorithm for the automatic extraction of axons from fluorescent confocal microscopy images was proposed. This method relies on several steps to perform the extraction: filament enhancement, binarization, skeletonization and gap filling. Due to the voxel anisotropy of our images, the filament enhancement step is performed on each 2D slice separately while the extraction (skeleton and gap filling) is performed in 3D.

The method performance was tested on 12 real 3D images and the results quantitatively evaluated by calculating the RMSE between the tracing done by an experienced biologist and the automatic tracing obtained by our method. The good results obtained in the validation show the potential use of this technique in helping biologists extract axonal trees from confocal microscope images. This is the first step necessary if one intends to perform a morphological analysis of axons.

In the future, we intend to improve the quantitative evaluation of the method and to work on the detection of bifurcation points, end points and other features of the axons. Moreover, we plan on integrating this method along with others in a software designed to help biologists perform morphological analyses of axons in fluorescent confocal microscopy images.

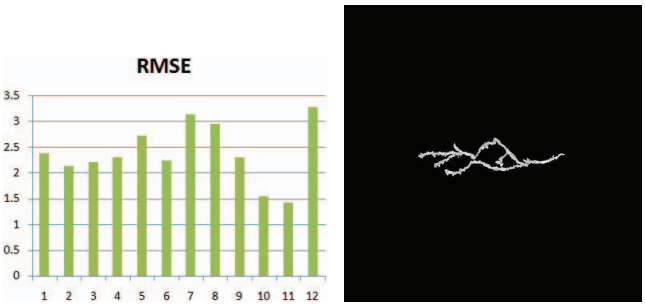



**Fig. 7**: RMSE voxel error of a set of 12 extracted axonal trees when compared to the ground truth (left) and one extracted axon in 3D (right).

## 5. REFERENCES

[1] *Y Zhang, X Zhou, J Lu, J Lichtman, D Adjeroh and S Wong*. 3D Axon Structure Extraction and Analysis in Confocal Fluorescence Microscopy Images. Neural Computation, August 2008, Vol. 20, No. 8, Pages 1899-1927.

[2] *J Wang, X Zhou, J Lichtman, SF Chang and S Wong*. Dynamic Local Tracing from 3D Axon Curvilinear Structure Detection from Microscopic Image Stack. In 4th IEEE International Symposium on Biomedical Imaging: From Nano to Macro, 2007.

[3] *H Peng, Z Ruan, D Atasoy and S Sternson*. Automatic Reconstruction of 3D Neuron Structures Using a Graph-Augmented Deformable Model. ISMB 2010, Vol. 26, pages i38-i46.

[4] *S Basu, A Aksel, B Condron and S T Acton*. Tree2Tree: Neuron segmentation for generation of neuronal morphology, In 2010 IEEE International Symposium on Biomedical Imaging: From Nano to Macro.

[5] *A F Frangi, W J Niessen, K L Vincken and M A Viergever*. Multiscale vessel enhancement filtering. Medical Image Computing and Computer-Assisted Intervention MICCAI, 98.

[6] *M H F Wilkinson and M A Westenberg*. Shape Preserving Filament Enhancement Filtering. Medical Image Computing and Computer-Assisted Intervention MICCAI, 2001.

[7] *N Otsu*. A threshold selection method from gray-level histograms. IEEE Trans. Sys., Man., Cyber. 9: 6266. doi:10.1109/TSMC.1979.4310076(1979).

[8] *L Risser, F Plouraboue, X Descombes*. Gap filling of 3-D microvascular networks by tensor voting. IEEE Trans Med Imaging. 2008 May;27(5):674-87.